

1 **Improving Runoff Simulation in the Western United States with**
2 **Noah-MP and VIC**

3 Lu Su^{a,b}, Dennis P. Lettenmaier^b, Ming Pan^a, Benjamin Bass^c

4 a Center for Western Weather and Water Extremes, Scripps Institution of Oceanography,
5 University of California, San Diego, United States

6 b Department of Geography, University of California, Los Angeles, United States

7 c Department of Atmospheric and Oceanic Sciences, University of California, Los Angeles,
8 United States

9 Correspondence: Dennis P. Lettenmaier (dlettenm@ucla.edu)

10 **Abstract**

11 Streamflow predictions are critical for managing water resources and for
12 environmental conservation, especially in the water-short Western U.S. Land Surface
13 Models (LSMs), such as the Variable Infiltration Capacity (VIC) model and the Noah-
14 Multiparameterization (Noah-MP) play an essential role in providing comprehensive
15 runoff predictions across the region. Virtually all LSMs require parameter estimation
16 (calibration) to optimize their predictive capabilities. Here, we focus on the
17 calibration of VIC and Noah-MP models at a 1/16° latitude-longitude resolution
18 across the Western U.S. We first performed global optimal calibration of parameters
19 for both models for 263 river basins in the region. We find that the calibration
20 significantly improves the models' performance, with the median daily streamflow
21 Kling-Gupta Efficiency (KGE) increasing from 0.37 to 0.70 for VIC, and from 0.22 to
22 0.54 for Noah-MP. In general, post-calibration model performance is for watersheds
23 with relatively high precipitation and runoff ratios, and at lower elevations. At a
24 second stage, we regionalize the river basin calibrations using the donor-basin method,
25 which establishes transfer relationships for hydrologically similar basins, via which

26 we extend our calibration parameters to 4,816 HUC-10 basins across the region.
27 Using the regionalized parameters, we show that the models' capabilities to simulate
28 high and low flow conditions are substantially improved following calibration and
29 regionalization. The refined parameter sets we developed are intended to support
30 regional hydrological studies and hydrological assessments of climate change impacts.

31

32 **1. Introduction**

33 Streamflow predictions play a key role in water and environmental management,
34 especially in the water-stressed Western U.S. (WUS). In the short term, these
35 predictions provide early warnings for impending flood events, thereby enabling
36 timely preparation and response to mitigate immediate flood risk and damages
37 (Maidment, 2017). They also serve as crucial input for managing reservoirs
38 effectively for water supply (Raff et al., 2013), hydroelectric power generation
39 (Boucher & Ramos, 2018), and river navigation (by providing a basis for predicting
40 water levels) (Federal Institute of Hydrology, 2020). In the longer term, streamflow
41 predictions enable water utilities and agencies to plan water distribution within and
42 across multiple uses—urban, agricultural, and industrial—which is especially vital
43 during drought conditions when efficient water use becomes a necessity (Anghileri et
44 al., 2016;). Streamflow predictions also aid in understanding and foreseeing the
45 impacts of climate change on water systems, thereby informing adaptive strategies for
46 water resource management. Thus, in both short and longer-term contexts, streamflow
47 predictions are an important tool for promoting sustainable water practices and
48 resilience to water-related challenges.

49 Streamflow predictions are derived via a synthesis of hydrometeorological data,
50 statistical methodologies, and computational modeling. Direct measurement of runoff
51 is an important element of this process, however it is only possible in river basins with

52 well-developed observational infrastructure (Sharma and Machiwal, 2021). This
53 limitation leaves vast areas, often critical to water resource management and
54 climatology, without direct runoff observations on which to base streamflow
55 predictions. As an alternative, Land Surface Models (LSMs) can be used to simulate
56 streamflow. LSMs typically are forced with air temperature, precipitation and other
57 surface meteorological variables. By integrating climatic, topographic, and land-use
58 information, they can fill streamflow observation gaps and provide comprehensive,
59 spatially distributed runoff predictions (Fisher and Koven, 2020). The capabilities of
60 LSMs equip us with the necessary tools to produce streamflow predictions that can be
61 used to prepare for severe weather conditions, form the basis for water resource
62 management, and inform water management associated with our evolving climate.
63 These benefits hold true irrespective of the limitations associated with direct
64 streamflow observations. Through off-line simulations and reconstructions, LSMs
65 enable us to gain insights into land surface hydrology at various scales - regional,
66 continental, and global.

67 Parameterizations of the underlying hydrological processes vary across different
68 LSMs, but virtually all models require some level of parameter estimation based on
69 historical observed streamflow data at forecast point, to ensure trustworthy
70 predictions throughout the region (Beven,1989; Troy et al., 2008; Gong et al., 2015).
71 In cases where observations don't exist, parameters can be transferred from river
72 basins where they do (Arsenault and Brissette, 2014). In cases where observations do
73 exist but aren't current, shorter records of historical streamflow data can be used for
74 model calibration and subsequently streamflow predictions can be produced using
75 meteorological forcings for more recent periods when streamflow data aren't
76 available.

77 Implementation of hydrological models for the above purposes usually involves

78 calibration of model parameters using streamflow observations, which are more
79 readily available than other model prognostic variables like soil moisture or
80 evapotranspiration (Demaria et al., 2007; Gao et al., 2018; Troy et al., 2008; Yadav et
81 al., 2007). Calibration has always been a critical and evolving component of
82 hydrologic model application, and has been improved by advances in model
83 parameterization, enhanced spatial resolution providing more detailed and accurate
84 spatial information, improved soil/vegetation data, meteorological inputs, and training
85 data. Furthermore, advances in calibration methods and computing power have
86 facilitated regional approaches to model calibration, and inclusion of multiple
87 hydrologic models. Previous studies mostly focus on a single hydrologic model due to
88 computational constraints (e.g., Mascaro et al. (2023), Sofokleous et al. (2023), and
89 Gou et al. (2020)). However, we incorporate two models to address structural model
90 uncertainty and to ensure broader applicability of the calibration methods we employ.

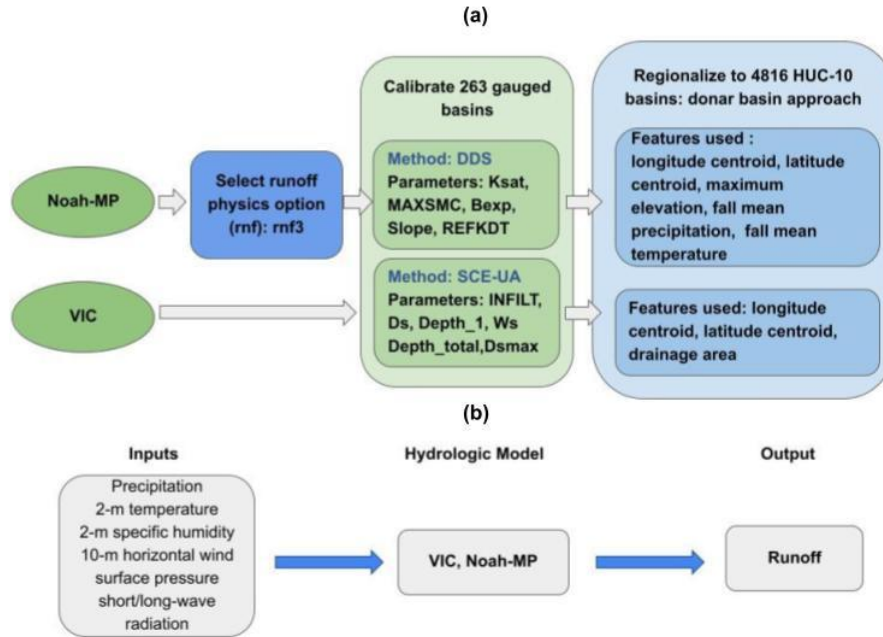
91 The Variable Infiltration Capacity (VIC, Liang et al. (1994)) model and Noah-
92 Multiparameterization (Noah-MP, Niu et al. (2011)), which we use here, are widely
93 used hydrologic models both in the U.S. and globally, as highlighted by Mendoza et al.
94 (2015) and Tangdamrongsub (2023). Many previous implementations of VIC for the
95 Western United States (WUS) have been based on the Livneh et al. (2013) data set,
96 and its predecessor, Maurer et al. (2002), which performed initial calibrations across
97 the region. In the case of Noah-MP, Bass et al. (2023) performed manual calibration
98 across the region. Neither of these implementations, however, employs globally
99 optimized calibration, as we do here.

100 The process of calibration can be computationally demanding, and prior research
101 typically has focused on obtaining parameters appropriate to facilitating model
102 simulations that match observations as closely as possible at stream gauge locations
103 (Duan et al,1992; Tolson and Shoemaker, 2007). Most previous studies have

104 concentrated on a limited number of gauges/river basins and a single model (e.g.
105 Mascaro et al. (2023); Sofokleous et al. (2023); and Gou et al. (2020)). Here, we aim
106 to establish parameterizations for two LSMs -- VIC and Noah-MP across the entire
107 WUS. In doing so, we apply global optimization methods at the river basin level,
108 followed by a second stage regionalization.

109 The work we report here aims to develop calibration parameters for the VIC and
110 Noah-MP models that can be implemented at the catchment (Hydrologic Unit Code or
111 HUC) 10 level across the region. We explore and elucidate (i) the choice of physical
112 parameterizations and calibration of land surface parameters, (ii) extension of these
113 calibrated parameters to areas without gauges, and (iii) factors that influence
114 calibration efficiency and LSM performance using regional parameter estimates.
115 Following this introduction, Section 2 describes our calibration basins, the hydrologic
116 models used, and the forcing dataset. The framework of our procedures is illustrated
117 in Figure 1. Section 3 provides an in-depth exploration of the calibration process. In
118 the case of Noah-MP, which offers multiple runoff generation (physics) options, our
119 initial step involves choosing the most effective runoff parameterization option.
120 Following this, we perform the calibration of land surface parameters. In the case of
121 the VIC model, the runoff parameterization scheme is predetermined, so we
122 commence immediately with calibration at 263 river basins across our region. Our
123 second stage regionalization (section 4) extends the calibrated parameters to ungauged
124 basins using the technique known as the donor basin method, as implemented by Bass
125 et al. (2023). In Section 5, we evaluate both flood and low flow simulation skills both
126 pre- and post-calibration, and following regionalization. Finally, following discussion
127 and interpretation (section 6) section 7 presents conclusions, encapsulating the
128 insights and implications of our study.

129



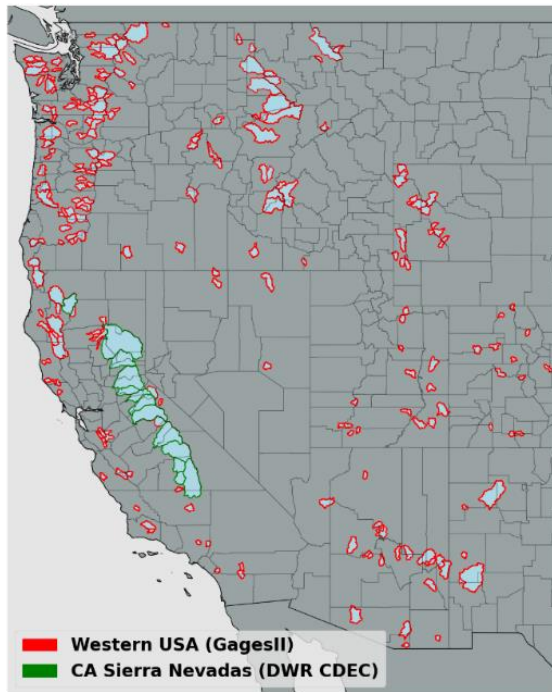
130

131 Figure 1 (a) framework of the calibration and regionalization processes adopted
 132 in this study. (b) model simulation inputs and output.

133 **2. Study basins, land surface models and forcing dataset overview**

134 **2.1 Study Basins**

135 We selected 263 river basins distributed across the WUS for calibration of the
 136 two models. Most of the basins were from USGS Gages II reference basins (Falcone
 137 2011) which have minimum upstream anthropogenic effects such as dams and
 138 diversions. Among these basins, our selection criteria included having at least 20
 139 years of record, and a minimum drainage area of 144 square kilometers, which is the
 140 size of four model grid cells. In addition to 250 Gages II reference stations, we
 141 included 13 basins located in California's Sierra Nevada for which naturalized flows
 142 (effects of upstream reservoir storage and/or diversions removed) are available from
 143 the California Department of Water Resources (2021). The locations of the 263 basins
 144 are shown in Figure 2. We used the most recent 20-year period of streamflow
 145 observations for calibration in each of the 263 basins.



146

147 Figure. 2. 263 river basins for which calibration was performed. The Gages II
148 reference basins are delineated with red boundaries and the CA Sierra Nevada basins
149 with green boundaries.

150 2.2 Land Surface Models

151 The two models we used (VIC and Noah-MP) were chosen due to their broad
152 application and proven effectiveness in hydrological simulations. The VIC model is
153 renowned globally for its success in runoff simulation, as evidenced by studies such
154 as Adam et al. (2003 & 2006), Livneh et al. (2013), and Schaperow et al. (2021).
155 Conversely, Noah-MP, though relatively newer, forms the hydrologic core of the U.S.
156 National Water Model (NWM) and is increasingly used both within the U.S. and
157 abroad.

158 Our selection is further reinforced by a study conducted by Cai et al. (2014),
159 which assessed the hydrologic performance of four LSMs in the United States using
160 the North American Land Data Assimilation System (NLDAS) test bed. This study

161 highlighted Noah-MP's proficiency in soil moisture simulation and its strong
162 performance in Total Water Storage (TWS) simulations, while recognizing VIC's
163 capabilities in streamflow simulations.

164 Our choice of models also was informed by the varying levels of complexity
165 these two models offer in conceptualizing the effects of vegetation, soil, and seasonal
166 snowpack on the land surface energy and water balances (refer to Table 1 for more
167 details). VIC and Noah-MP employ different parameterizations for various
168 hydrological processes, such as canopy water storage, base flow, and runoff. Noah-
169 MP features four runoff physics options (see Table 1). It utilizes four soil layers, each
170 with a fixed depth. In contrast, the VIC model, with its variable infiltration capacity
171 approach (Liang et al., 1994), uses up to three soil layers per grid cell with variable
172 depths, providing flexibility in modeling soil moisture dynamics. The unique runoff
173 generation methodologies of each model are particularly pertinent for capturing the
174 diverse hydrological characteristics of the WUS.

175 The calibrated parameters we develop here for both models will provide future
176 researchers with essential tools for comprehensive hydrological analysis across the
177 WUS. Utilizing these two distinct models, each with unique strengths and methods,
178 will facilitate thorough exploration of the WUS's varied hydrological characteristics,
179 and response of the watersheds in the region to climate change, as well as
180 implementation of improved streamflow forecast methods. Our results will help to
181 facilitate a deeper understanding of hydrological processes and spatial variability
182 across the entire WUS region.

183 In our implementation of both models, we accumulated runoff over each of the
184 calibration watersheds. We chose not to implement the channel routing schemes of
185 either model since their impact on daily streamflow simulations is small given the
186 relatively small size of most of the basins. This aligns with earlier research (e.g., Li et

187 al. 2019). However, in both the case of VIC and Noah-MP, the output of our
188 simulations (runoff) could be used as input to routing models, such as those that are
189 options in the implementation of both models. We describe below the particulars of
190 the two models.

191 **2.2.1 VIC**

192 VIC is a macroscale, semi-distributed hydrologic model (described in detail by
193 Liang et al 1994) that determines land surface moisture and energy states and fluxes
194 by solving the surface water and energy balances. VIC is a research model and in its
195 various forms it has been employed to study many major river basins worldwide (e.g.
196 Adam et al 2003 & 2006; Livneh et al 2013; Schaperow et al 2021). This model
197 enjoys a broad user community — as per the citation index Web of Science, the initial
198 VIC paper has been referenced more than 2600 times, with contributing authors
199 spanning at least 56 different countries (Schaperow et al 2021). We obtained initial
200 VIC model parameters from Livneh et al 2013, who validated model discharges over
201 major CONUS river basins. The origins of the soil and land cover data are outlined in
202 Table 1. The version of the VIC model implemented here is 4.1.2, and it operates in
203 energy balance mode. We selected VIC 4.1.2 for two key reasons: First, our initial
204 parameters were based on Livneh et al. (2013), who validated model discharges over
205 major CONUS river basins using this model version. Second, in a preliminary
206 assessment of snow water equivalent (SWE) simulation skills at select SNOTEL sites
207 across the WUS, we found that VIC 4.1.2 demonstrated superior performance
208 compared to VIC 5 (see Figure S1). This finding, coupled with our research group's
209 extensive experience and proven results with VIC 4.1.2, informed our decision to use
210 this version.

211 **2.2.2 Noah-MP**

212 Noah-MP was originally designed as the land surface scheme for numerical
213 weather prediction (NWP) models like the Weather Research and Forecasting (WRF)
214 regional atmospheric model. Currently, it's being utilized for physically based,
215 spatially-distributed hydrological simulations as a component of the National Water
216 Model (NWM) (NOAA, 2016). It enhances the functionalities of the Noah LSM (as
217 per Chen et al., 1996 and Chen and Dudhia, 2001) previously used in NOAA's suite of
218 numerical weather prediction models by offering multiple options for key processes
219 that control land-atmosphere transfers of moisture and energy. These include surface
220 water infiltration, runoff, evapotranspiration, groundwater movement, and channel
221 routing (see Niu et al., 2007; 2011). The model has been widely used for forecasting
222 seasonal climate, weather, droughts, and floods not only across the continental United
223 States (CONUS) but also globally (Zheng et al., 2019). We utilized the most current
224 version (WRF-HYDRO 5.2.0)

225 **2.3 Forcing Dataset**

226 We ran both models at a 3-hour time step and at $1/16^\circ$ latitude–longitude spatial
227 resolution. The forcings were the gridded observation dataset developed by Livneh et
228 al (2013) and extended to 2018 by Su et al (2021) (hereafter referred to as L13). This
229 data set spans the period from 1915 to 2018. For the VIC model, the L13 dataset
230 provided daily values of precipitation, maximum and minimum temperatures, and
231 wind speed (additional variables used by VIC including downward solar and
232 longwave radiation, and specific humidity, are computed internally using MTCLIM
233 algorithms as described by Bohn et al. (2013)). The Noah-MP model, on the other
234 hand, necessitated additional meteorological data such as specific humidity, surface

235 pressure, and downward solar and longwave radiation, in addition to precipitation,
 236 wind speed, and air temperature. We used the MTCLIM algorithms, as detailed by
 237 Bohn et al. (2013), to calculate specific humidity and downward solar radiation. We
 238 employed the Prata (1996) algorithm to compute the downward longwave radiation.
 239 Additionally, we deduced surface air pressure by considering the grid cell elevation in
 240 conjunction with standard global pressure lapse rates. Following this, we transitioned
 241 the daily data to hourly metrics using a cubic spline to interpolate between Tmax and
 242 Tmin, and derived other variables using the methods explained by Bohn et al. (2013).
 243 Lastly, we distributed the daily precipitation evenly across three hourly intervals.

244 We used a 3-hour simulation timestep given numerical considerations with
 245 Noah-MP (which don't affect VIC, however for consistency we used a 3-hour
 246 timestep for VIC as well. Despite the fact that precipitation in particular was available
 247 daily (and hence apportioned equally to 3-hour timesteps) resolving the diurnal cycle
 248 is sometimes important in the case of snow (accumulation and ablation) processes
 249 which vary diurnally.

250 Table 1. Overview of hydrologic model components and parameter data sources.

MODEL	SNOW ACCUMULATION AND MELT	MOISTURE IN THE SOIL AND COLUMN/SURFACE RUNOFF	BASE FLOW	CANOPY STORAGE	VEGETATION DATA	SOIL DATA
VIC (V4.1.2)	Two-layer energy–mass balance model	Infiltration capacity function. Vertical movement of moisture through soil follows 1D Richards equation.	A function of the soil moisture in the third layer. Linear below a soil moisture threshold and becomes nonlinear above that threshold. [Liang et al., 1994]	Mosaic representation of different vegetation coverages at each cell.	University of Maryland 1-km Global Land Cover Classification (Hansen et al. 2000)	1-km STAT SGO database (Miller and White 1998).
NOAH-MP (WRF-HYDRO 5.2.0)	Three-layer energy–mass balance model that represents percolation	(1) TOPMODEL-based runoff scheme (2) Simple TOPMODEL-based runoff scheme with an equilibrium	Simple groundwater (hereafter SIMGM) [Niu et al., 2007]. Similar to SIMGM, but with a sealed bottom of the soil column [Niu et al.,	Semi-tile approach for computing longwave, latent heat, sensible heat and ground heat	MODIS 30-second Modified IGBP 20-category land cover product	1-km STAT SGO database (Miller and White

	, retention, and refreezing of meltwater within the snowpack.	water	table	2005]	fluxes	1998).
		(hereafter SIMTOP)				
		(3) Infiltration-excess-based surface runoff scheme		Gravitational free-drainage subsurface runoff scheme [Schaake et al., 1996]		
		(4) BATS runoff scheme, which parameterized surface runoff as a 4th power function of the top 2 m soil wetness (degree of saturation)		Gravitational free drainage [Dickinson et al.,1993]		

251 **3. Model calibration**

252 **3.1 Calibration methods**

253 The initial step in our calibration effort was to optimize the land surface
 254 parameters of the two models for the 263 WUS basins. These parameters, primarily
 255 soil properties which can exhibit a substantial degree of uncertainty, were iteratively
 256 updated via hundreds of simulations to accurately reflect streamflow conditions in
 257 each basin.

258 Our focus on calibrating soil-related parameters was based on their critical role
 259 in runoff generation. In this respect, we focused on key processes including
 260 infiltration, soil moisture storage, and groundwater recharge. The calibration of
 261 parameters that control these processes was prioritized to improve the representation
 262 of soil-water interactions, a major driver of runoff variability in the region. Given the
 263 importance of snow processes across much of the region, we conducted snow
 264 simulation verification at 20 Snow Telemetry (SNOTEL) (Natural Resources
 265 Conservation Service, 2023) sites across WUS. Our assessment (see Figure S1)
 266 indicated that the existing parameterizations for snow processes in both models
 267 reproduced observed SWE well across our study region.

268 Prior to calibration, we conducted a sensitivity analysis to identify the most

269 influential parameters for streamflow simulation in both models. We also drew on
270 insights from previous research in this respect (Mendoza et al. 2015; Hussein 2020;
271 Shi et al. 2008; Holtzman et al., 2020; Bass et al., 2023; Schaperow et al., 2023). We
272 then performed a sensitivity analysis, focusing on how variations in the most sensitive
273 parameters impacted Kling-Gupta Efficiency (KGE; Gupta et al., 2009). Based on
274 these analyses, we chose to calibrate six parameters for the VIC model and five for
275 the Noah-MP model (Table 2). For each parameter, we defined a physically viable
276 range (refer to Table 2), drawing from values utilized in prior studies (Cai et al. 2014;
277 Mendoza et al. 2015; Hussein 2020; Shi et al. 2008; Gochis et al., 2019; Holtzman et
278 al., 2020; Lahmers et al. 2021; Bass et al., 2023; Schaperow et al., 2023).

279 In recent years, the development of hydrologic model calibration has evolved
280 from manual, trial-and-error approaches to advanced automated techniques. This has
281 included a shift towards global optimization methods, notably the Shuffled Complex
282 Evolution algorithm (SCE-UA; Duan et al., 1992). Typically, SCE-UA has been
283 applied to computationally efficient models (simulation time often on the order of a
284 few minutes or less; see e.g., Franchini et al. (1998)). However, its application
285 becomes less practical with more recent distributed hydrologic models such as the
286 Noah-MP which require longer simulation times. To address these computational
287 challenges, Tolson and Shoemaker (2007) introduced the Dynamically Dimensioned
288 Search (DDS) algorithm, tailored for complex, high-dimensional problems. DDS is
289 more computationally efficient than SCE-UA, and we therefore used it for our
290 Noah-MP calibrations.

291 To assure that the parameter sets we estimated weren't dependent on the
292 optimization method, we conducted a comparison between SCE-UA and DDS for
293 calibrating VIC across 20 randomly chosen basins. We found that the DDS algorithm
294 achieved optimal calibration with fewer iterations (typically around 3000 iterations vs

295 only about 250 for DDS). The parameter sets identified were nearly identical,
 296 affirming our decision to use distinct algorithms tailored to the computational
 297 demands of each model.

298 For both models, our objective function was the KGE metric for daily
 299 streamflow. KGE is a widely used performance measure because of its advantages in
 300 orthogonally considering bias, correlation and variability (Knoben et al., 2019). KGE
 301 = 1 indicates perfect agreement between simulations and observations; KGE values
 302 greater than -0.41 indicate that a model improves upon the mean flow benchmark
 303 (Konben et al., 2019).

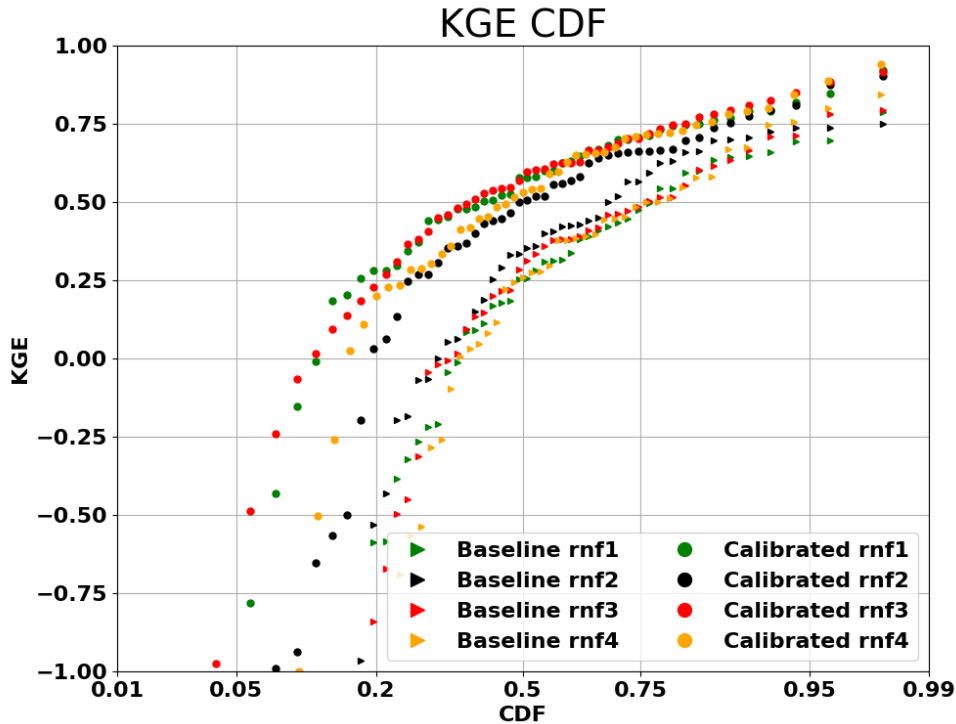
304 TABLE 2. Calibration methods, parameters and modifications to their initial
 305 default values evaluated in the calibration.

Model	VIC		Noah-MP	
Calibration Method	SCE-UA		DDS	
Iterations	3000		250	
Calibrated Parameter	Variable Infiltration Curve Parameter (INFILT)	0.001 – 0.4 (Shi et al.,2008)	Saturated Hydraulic Conductivity (Ksat)	2×10^{-9} to 0.07 (Cai et al.,2014)
	Baseflow parameter (Ds)	0.001 – 1.0 (Shi et al.,2008)	Saturation soil moisture content (MAXSMC)	0.1 to 0.71 (Cai et al.,2014)
	Thickness of Soil in Layer 1 (Depth_1)	0.01 – 0.2 (Shi et al.,2008)	Pore size distribution index (Bexp)	1.12 to 22 (Cai et al.,2014; Gochis et al.,2019)
	Total thickness of soil column (Depth_total)	0.6 – 3.5 (Shi et al.,2008)	Linear scaling of “openness” of bottom drainage boundary (Slope)	0.1-1 (Lahmers et al 2021)
	Max velocity parameter of baseflow (Dsmax)	0.001 – 30 (Schaperow et al.,2023)	Parameter in surface runoff (REFKDT)	0.1-10 (Lahmers et al 2021)
	Fraction of max	0.001 – 1		

soil moisture (Shi et
where nonlinear al.,2008)
baseflow occurs
(Ws)

306 **3.2 Noah-MP parameterization**

307 As specified in Table 1, Noah-MP has four runoff and groundwater physics
308 options (rnf). Initially, we adopted the options that are incorporated in the NWM, as
309 elaborated in Gochis et al. (2020). Before we could proceed with calibrating Noah-
310 MP for all the WUS basins, it was necessary to determine suitable rnfs. To streamline
311 computational time, we initially selected 50 basins randomly from the total of 263
312 from which we created four experimental groups. Each group employed a different
313 rnf option. We applied the DDS method to these groups and compared the cumulative
314 distribution functions (CDF) of their baseline and calibrated KGEs (Figure 3). From
315 this figure, it's apparent that the KGE improved post-calibration for all four rnfs.
316 Notably, rnf3, also known as free drainage, exhibited the most substantial
317 performance enhancement after calibration. As a result, we chose to continue using
318 this option which is incorporated in the NWM. Nonetheless, it's worth noting that the
319 use of different options for different basins—a feature currently not utilized in Noah-
320 MP or WRF-Hydro—could potentially result in improved overall model performance.



321

322 Figure 3. Streamflow performance (KGE of daily streamflow simulations) of
 323 different Noah-MP runoff generation options across 50 (of 263) randomly selected
 324 basins. The performances are shown for both baseline and calibrated simulations.

325 3.3 Calibration of gauged basins

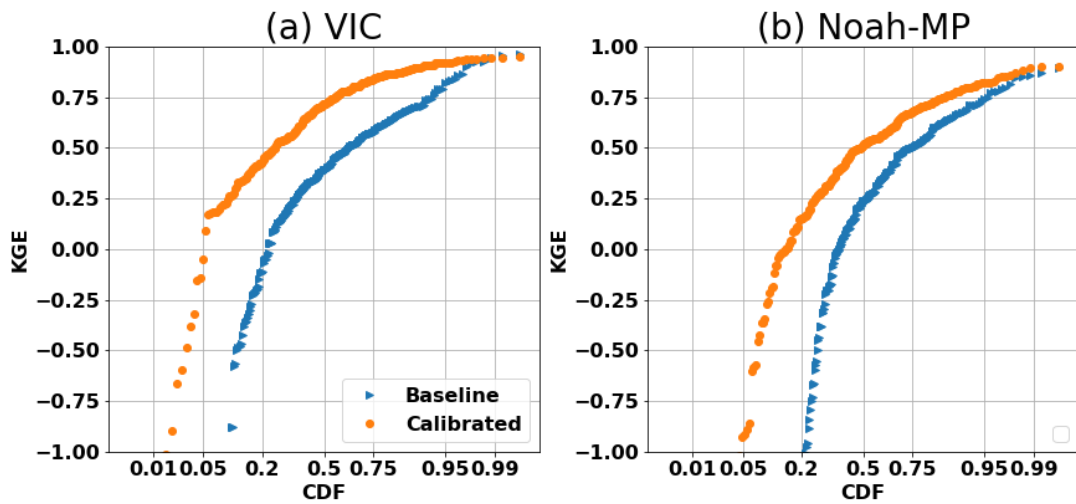
326 Following the selection of the most effective set of runoff generation options
 327 across the domain, we estimated model parameters for all 263 basins. The
 328 comparative performance of the models, before and after calibration, is shown in
 329 Figure 4. It's apparent from the figure that both Noah-MP and VIC have significantly
 330 enhanced their daily streamflow simulation skills post-calibration. After calibration,
 331 the median KGE of Noah-MP improved from 0.22 to 0.54, and the VIC's median
 332 KGE increased from 0.37 to 0.70. When contrasting the two models, we observed that
 333 VIC outperformed Noah-MP both pre- and post-calibration. One possible explanation
 334 could be that the baseline VIC parameters were taken from Livneh et al. (2013), and
 335 these parameters had already been validated and adjusted for major U.S. basins

336 (although not for our 263 basins specifically), while the Noah-MP parameters are
337 default values from NWM. Another possibility is inherent differences in the physics
338 of streamflow simulation between the two models (VIC primarily generates runoff via
339 the saturation excess mechanism), although that isn't the main focus of our research.

340 Following the calibration with data from the past 20 years, we performed a test
341 where we calibrated the streamflow using the first 10 years of data and validated with
342 the subsequent 10 years of data. This test revealed that the KGE distribution from the
343 10-year calibration is similar to that from the 20-year data. The median KGE values
344 for VIC and Noah-MP after calibration with 10 years of observations were 0.52 and
345 0.69, respectively. Correspondingly, the median KGEs during the validation period
346 were 0.50 and 0.68, respectively, which are only slightly lower. These comparisons
347 demonstrate general consistency over time in the performance of the calibrated
348 parameters.

349 To validate the robustness of our calibration methodology, we calculated
350 alternative (to KGE) performance metrics, specifically Nash-Sutcliffe Efficiency
351 (NSE) and bias. Our analyses, detailed in Figures S2&3, revealed significant
352 enhancements in model performance as measured by these metrics. The observed
353 improvements across multiple evaluation criteria affirm the efficacy of our calibration
354 process, and in particular that the performance of our procedures is not contingent
355 upon the choice of evaluation metrics.

356



357

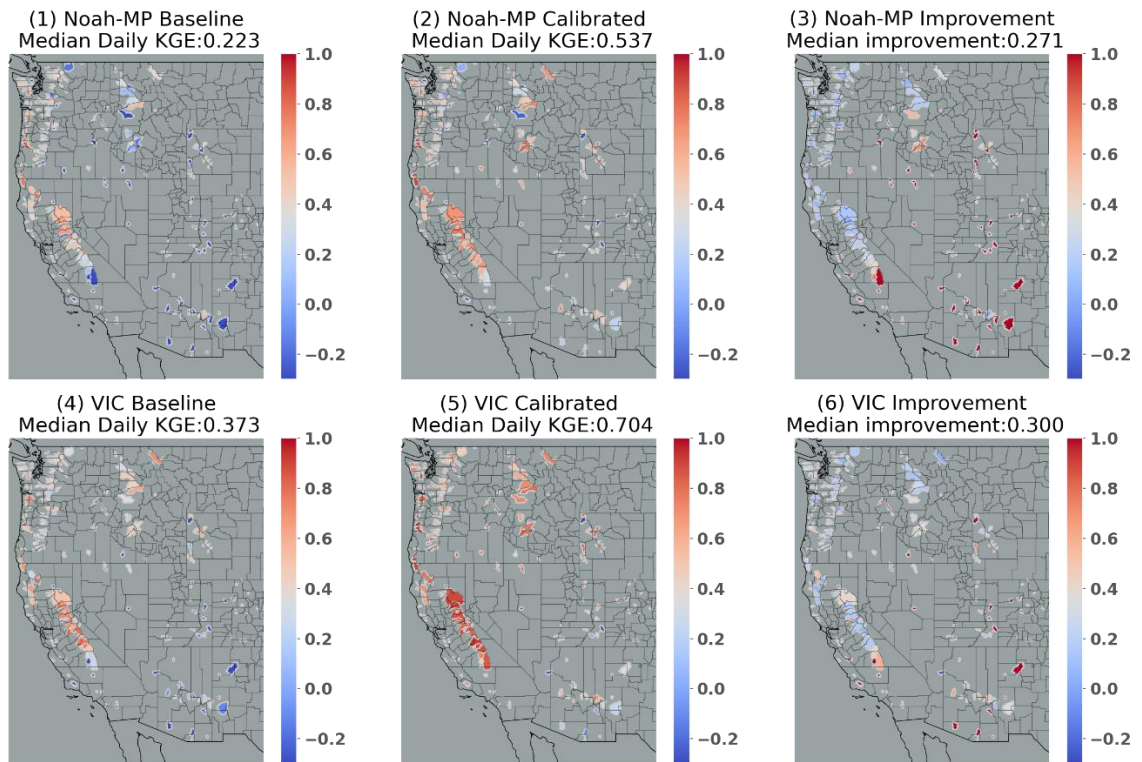
358 Figure 4. Cumulative Distribution Function (CDF) plot of the daily streamflow
 359 KGE for (a) VIC and (b) Noah-MP, comparing baseline and calibrated runs across all
 360 263 basins.

361 We examined the spatial variability of daily streamflow KGE for Noah-MP and
 362 VIC, both before and after the calibration (see Figure 5). The highest baseline KGEs
 363 are along the Pacific Coast, in central to northern CA for both models. VIC's baseline
 364 KGE generally is high in the Pacific Northwest. Post-calibration improvements
 365 occurred for both models in most areas, especially in regions where the baseline KGE
 366 was low, such as southern CA and the southeastern part of the study region. Median
 367 improvements after calibration were 0.27 for Noah-MP and 0.30 for VIC.

368 We observed that basins displaying higher KGE values typically were more
 369 humid than those with lower KGE. To further delve into the relationship between
 370 KGE and basin characteristics, we explored correlations between KGE and 21
 371 different characteristics, including drainage area, elevation, seasonal/annual average
 372 temperature and precipitation, annual maximum precipitation, and seasonal/annual
 373 runoff ratio. Of these, 12 characteristics were statistically significantly correlated with
 374 the VIC KGE, including four seasonal and annual runoff ratios; mean precipitation in
 375 winter, spring, and fall; annual maximum precipitation; and minimum elevation.

376 Figure 6 shows scatterplots of eight representative characteristics. Apart from
377 minimum elevation and mean summer temperature, all other characteristics were
378 positively correlated with KGE. Typically, spring runoff ratio, annual runoff ratio,
379 mean annual max precipitation, and mean winter precipitation exhibited the highest
380 correlations with KGE. This implies that basins with higher runoff ratios (particularly
381 in spring), higher precipitation (especially maximum precipitation), lower summer
382 temperature, and lower elevation are more likely to exhibit strong VIC performance.
383 The same applies to Noah-MP, as indicated in Figure 7, although Noah-MP showed
384 relatively weaker correlations. Correlations between mean summer temperature and
385 mean fall precipitation and Noah-MP KGE weren't statistically significant.

386 The spatial distribution of the eight characteristics is qualitatively similar with
387 the KGE spatial distribution, as shown in Figure 8. Generally, basins with higher KGE
388 have higher characteristic values when the correlation is positive, and lower
389 characteristic values when the correlation is negative. As noted above, both models
390 show good baseline performance along the Pacific Coast, and in central to northern
391 CA (Figure 5). Those areas have high runoff ratios (specifically spring and annual)
392 and high mean winter precipitation. These features generally lead to runoff physics
393 that are dominated by the saturation-excess mechanism, which is well represented by
394 both VIC and Noah-MP. VIC's baseline KGE generally is high in the inland
395 Northwest which has somewhat lower runoff ratios and (relatively) deeper
396 groundwater tables. VIC's superior performance relative to Noah-MP may also be
397 because of its variable rather than fixed soil moisture depths (as is the case for Noah-
398 MP).



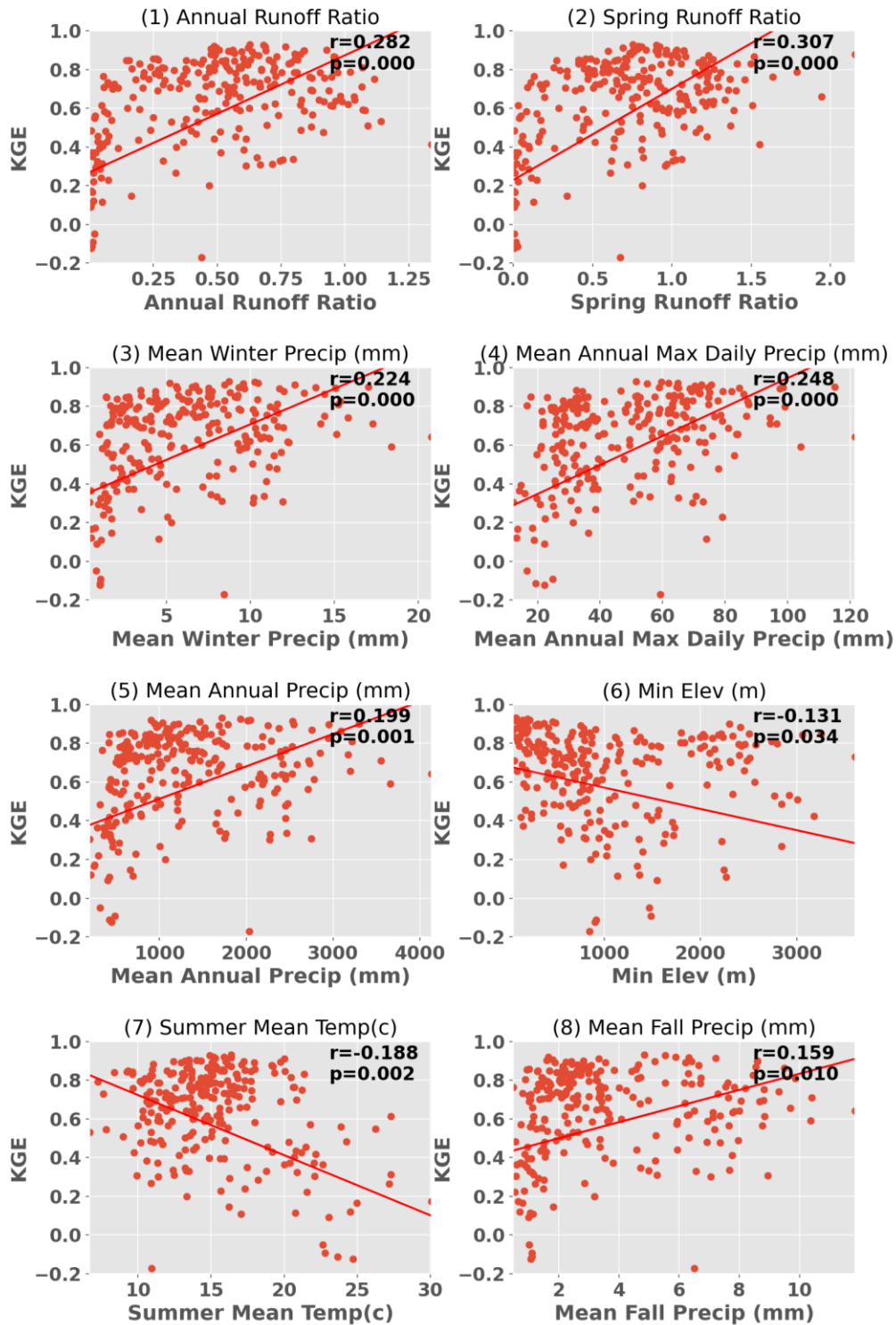
399

400 Figure 5. Spatial distribution of daily streamflow KGE for Noah-MP baseline (1);

401 calibrated Noah-MP (2); difference between calibrated and baseline Noah-MP (3);

402 VIC baseline (4); calibrated VIC (5); difference between calibrated and baseline VIC

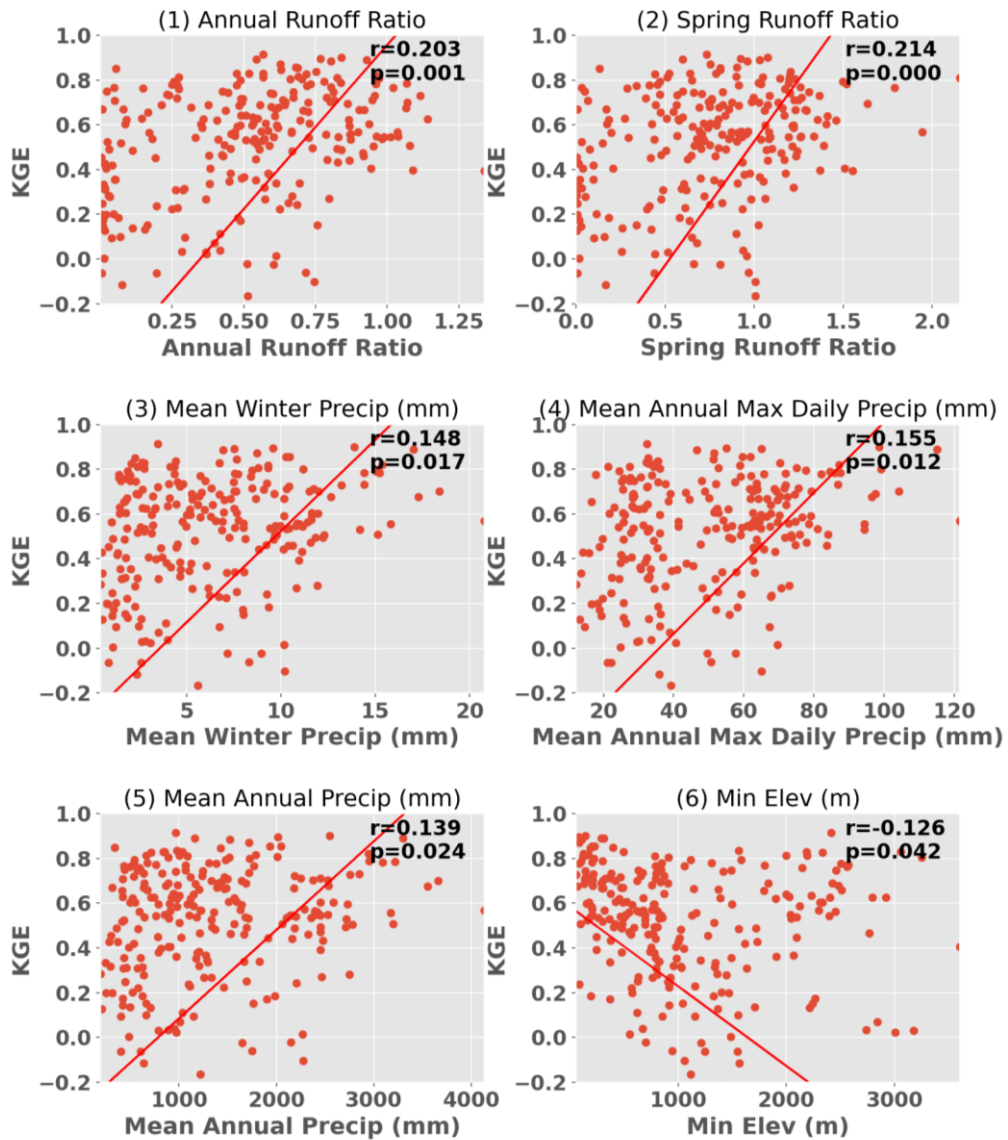
403 (6).



404

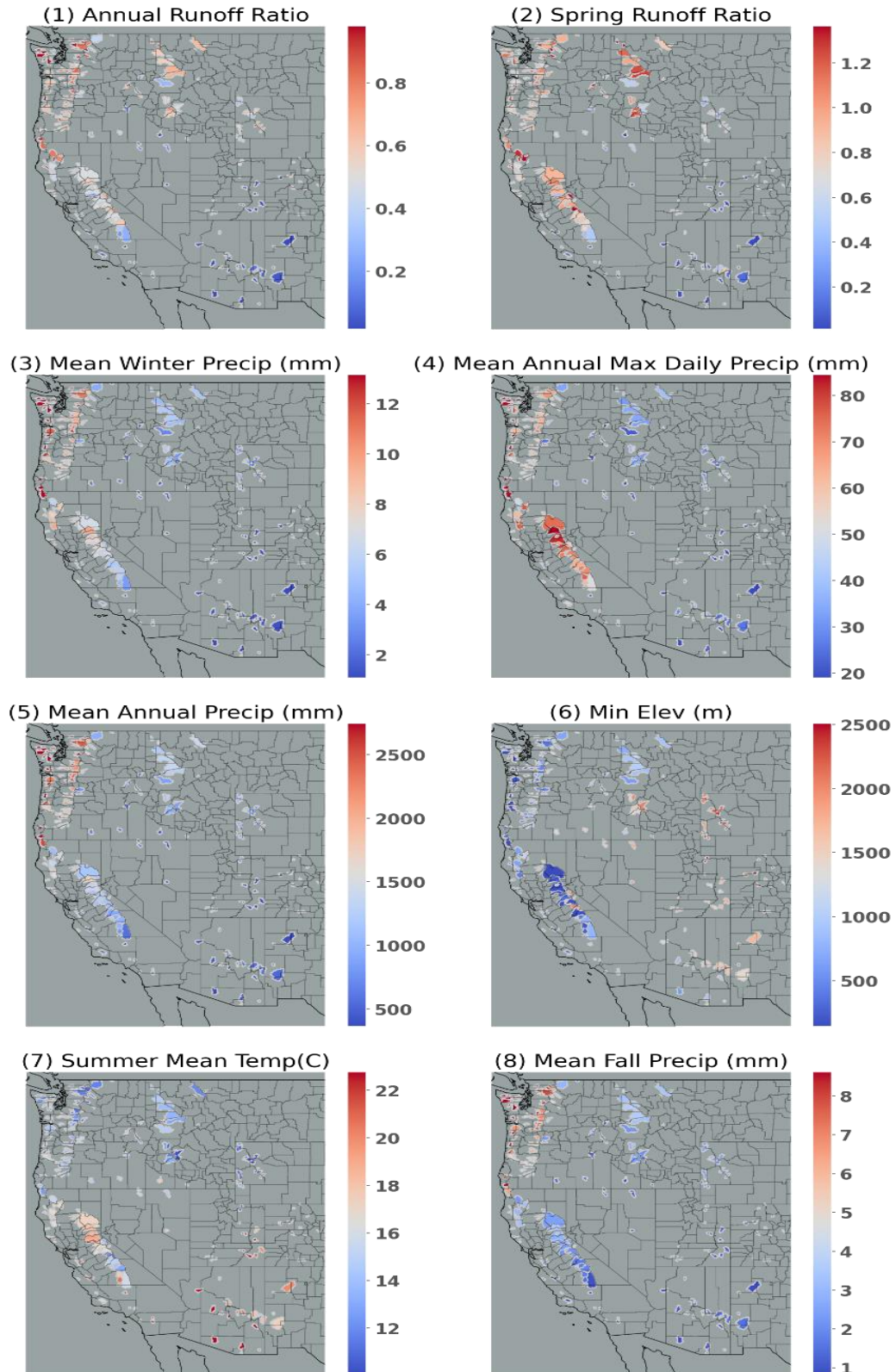
405

Figure 6. Scatterplots of VIC KGE in relation to significantly correlated
 406 characteristics. Each subplot indicates the corresponding Pearson correlation
 407 coefficients and the P-value.



408

409 Figure 7. Scatterplot of Noah-MP KGE in relation to significantly correlated
 410 characteristics. Each subplot indicates the corresponding Pearson correlation
 411 coefficients and the P-value.



412

413

Figure 8. Spatial distribution of characteristics that are statistically significantly

414

correlated with KGE. Note that all characteristics are significantly correlated with

415

VIC KGE whereas only (1)-(6) are significantly correlated with Noah-MP KGE.

416 **4. Regionalization**

417 To distribute parameters from the calibration basins to the entire region, we used
418 the donor-basin method as implemented in numerous previous studies (e.g., Arsenault
419 and Brissette (2014); Poissant et al. (2017); Razavi and Coulibaly (2017); Gochis et al.
420 (2019); Qi et al. (2021) and Bass et al. (2023). Following the calibration process, we
421 regionalized the parameters from gauged to ungauged basins based on a mathematical
422 assessment of the spatial and physical proximity between the gauged and ungauged
423 basins. We considered two primary methods for implementing the donor basin
424 approach. The first uses models calibrated to spatially continuous gridded runoff
425 metrics (Beck et al. 2015; Yang et al. 2019). The second approach, which we
426 ultimately adopted, calibrates models to individual gauges, then extends these
427 parameters to ungauged basins, based either on a statistical or mathematical similarity
428 measures (e.g., Arsenault and Brissette 2014; Razavi and Coulibaly 2017). Our
429 preference for the second method was guided by a key limitation of the first approach,
430 specifically it is limited to calibrating against runoff metrics, such as long-term mean
431 flow and flow percentiles, rather than streamflow time series.

432 In the donor-basin method, an ungauged basin inherits its land surface
433 parameters from the most similar gauged basin(s) (or the 'n' most similar gauged
434 basins). Here, we evaluated the similarity or proximity between gauged and ungauged
435 basins based on the similarity index SI as defined and used by Burn and Boorman
436 (1993) and Poissant et al. (2017):

$$437 \quad SI = \sum_{i=1}^k \frac{|X_i^G - X_i^U|}{\Delta X_i} \quad (1)$$

438 In Eq. 1, k stands for the total number of features considered, X_i^G represents the *i*th
439 feature of the gauged basin G, X_i^U is the *i*th feature of a specific ungauged basin, and
440 ΔX_i is the range of potential values for the *i*th feature, grounded in the data from the

441 gauged basins. This yields a unique value of SI for each gauged basin, contingent on
442 the specific ungauged basin it is compared with. Typically, gauged basins that exhibit
443 greater resemblance to the ungauged basin will have a smaller SI.

444 We assessed the donor-basin method's efficacy using a cross-validation approach,
445 where each gauged basin was treated as ungauged one at a time. The pseudo-
446 ungauged basin inherits its hydrological parameters from its three most similar
447 gauged basins, determined by SI. The parameters inherited are a weighted average
448 from the three donor basins. After testing one to five donor basins, we found that
449 using three donors yielded the best results. Thus, every basin inherits parameters from
450 the three most similar gauged basins in each simulation, offering a concise evaluation
451 of the donor-basin method's regionalization performance.

452 We used 18 basin-specific features in the donor basin method, detailed in Table
453 S1, calculated based on the forcings and parameters used in the study. For feature
454 selection in the donor-basin method, we adopted an iterative approach, explained in
455 detail in the following paragraph. Only basins with a KGE exceeding 0.3 were
456 considered, following previous studies suggesting that inclusion of poorly performing
457 basins can lower regionalization performance. We found that a KGE threshold of 0.3
458 resulted in a median performance improvement of 0.08 larger than did a KGE
459 threshold of 0, hence it was chosen. After screening, 223 basins were utilized in VIC
460 regionalization and 194 in Noah-MP regionalization. We note that the parameters used
461 for calibration and the features used to determine the similarity index in the
462 regionalization process are different. The physics that control the key hydrological
463 processes of the two models are different, so we explored their best regionalization
464 features separately.

465 To determine the most effective regionalization features from the 18 basin
466 characteristics listed in Table S1, we employed a systematic iterative approach. The

467 first iteration includes 18 simulations, each of which incorporates one of the 18
468 features. The feature that yielded the greatest increase in the median KGE across all
469 basins, based on leave-one-out cross validation, was then retained. In the second
470 iteration, we conducted 17 simulations, each combining the retained feature from the
471 first iteration with one of the remaining 17 features. This process was repeated
472 iteratively, reducing the number of features considered in each subsequent round, until
473 the addition of new features no longer resulted in an appreciable increase in median
474 KGE. The sequence of features shown in Figure 9 (also shown in Table S1) indicated
475 the importance of the features. This iterative approach ensured that each feature's
476 individual and combined contribution to model performance was thoroughly assessed.
477 It allowed us to identify a subset of features that, when used together, optimally
478 improved model accuracy. We recognize the potential existence of inter-feature
479 correlations that may exert a discernible influence on their collective efficacy when
480 utilized in combination.

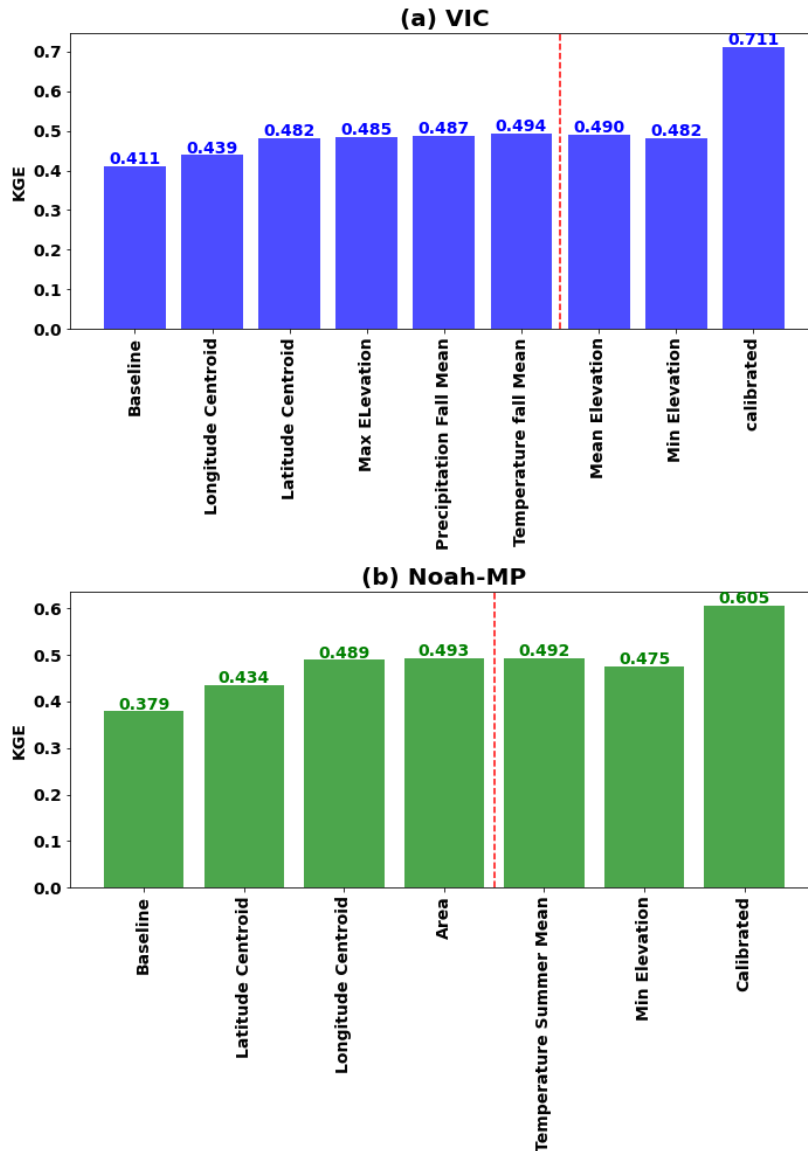
481 This procedure resulted in five features generated the best regionalization
482 performance for VIC (longitude centroid, latitude centroid, maximum elevation, fall
483 mean precipitation, and fall mean temperature). Three features were found to be best
484 for Noah-MP (latitude centroid, longitude centroid, and drainage area) (see Figure 9).
485 Among them, latitude and longitude are the common features that contribute the most
486 to regionalization when using the similarity index method. This suggests that
487 geographical similarities are the most important factor in parameter information
488 transfer from gauged to ungauged basins.

489 Upon evaluating the performance of baseline, calibrated, and regionalized
490 simulations, the respective median daily KGEs for the VIC model were found to be
491 0.41, 0.71, and 0.49. For the Noah-MP, these values were 0.38, 0.60, and 0.49 (refer
492 to Figures 9 & S4). These metrics are for basins that have a calibrated KGE greater

493 than 0.3 only, resulting in higher median KGEs than for all 263 basins (See Figure 4).
494 The KGE distribution also improved overall. It's noteworthy that the regionalization
495 improvement relative to baseline is higher for Noah-MP than for VIC. While VIC's
496 baseline and calibrated KGE skill distribution outperforms Noah-MP's, the
497 regionalized skills of Noah-MP and VIC are quite comparable. This observation might
498 be attributable to the constraints of the regionalization setup and could warrant future
499 investigation.

500 After optimizing the features and specific design of the donor-basin method,
501 parameters were regionalized to 4816 ungauged USGS Hydrologic Unit Code (HUC)
502 -10 basins across the WUS. HUCs are delineated and quality controlled by USGS
503 using high-resolution DEMs. For each of the 4816 HUC-10 basins, we calculated a
504 similarity index with the calibrated basins using the selected features. The three most
505 similar basins were identified as donor basins, and their weighted average parameters
506 were then adopted by the target HUC-10 basin. The final hydrologic parameters for
507 both VIC and Noah-MP for all WUS HUC-10 basins are shown in Figures S5&6.
508 The baseline HUC-10 parameters are shown in Figures S7&8.

509 Comparison of Figures S4-5 to Figures S6-7 makes it clear that the baseline
510 model parameters lack accuracy, and exhibit significant spatial uniformity where large
511 geographical regions share identical parameter values. For example, parameters such
512 as Ds and Soil_Depth1 in VIC show this uniformity. Furthermore, certain parameters,
513 such as SLOPE and REFKDT in Noah-MP, remain invariant across all spatial
514 domains, and don't reflect real-world conditions. Regionalization, improved the
515 parameters, leading to increased accuracy and strengthening of region-specific
516 characteristics.



517

518 Figure 9. Best regionalization features for (a) VIC and (b) Noah-MP. The final
 519 regionalization to ungauged basins of the WUS incorporated all features up to the
 520 point marked by the red line since the addition of further features doesn't improve
 521 KGE.

522 5. Evaluation of high and low flow simulation skill

523 Our primary calibration objective was to enhance the accuracy of daily
 524 streamflow simulations. However, to ensure the versatility of our parameter sets for
 525 research related to both floods and dry conditions, we also evaluate the models'
 526 capabilities in reproducing high and low streamflow. To understand the capabilities of

527 the two models in reconstructing high and low streamflow, we assessed their
528 performance across baseline, calibrated, and regionalized settings.

529 (a) Evaluation of high flow performance

530 We used the peaks-over-threshold (POT) method (Lang et al. 1999) to identify
531 extreme streamflow events as in Su et al (2023) and Cao et al. (2019, 2020). We first
532 applied the event independence criteria from USWRC (1982) to daily streamflow data
533 to identify independent events. We set thresholds at each basin that resulted in 3
534 extreme events per year on average. After selecting the flood events over the study
535 period based on the observation, we sorted the floods based on the return period and
536 then calculated the KGE of baseline, calibrated and regionalized floods. Figure S9
537 displays the associated CDF plots. The median KGE for baseline floods in Noah-MP
538 was 0.14, which rose to 0.37 post-calibration, and receded to 0.22 after
539 regionalization. For VIC, the flood KGE started at 0.11, increased to 0.41 after
540 calibration, and declined to 0.20 post-regionalization. As anticipated, these numbers
541 are lower than (all) daily streamflow skill due to our calibration target being daily
542 streamflow. Still, flood competencies experienced considerable enhancement,
543 surpassing the Noah-MP KGE benchmark of -0.41 found by Knoben et al. (2019).

544 (b) Evaluation of low flow performance

545 To assess low flow performance, we utilized the 7q10 metric. This hydrological
546 statistic, commonly adopted in water resources management and environmental
547 engineering, is the lowest 7-day average flow that occurs (on average) once every 10
548 years (EPA,2018). Scatterplots of 7q10 (Figure S10) showed high correlation between
549 our model's simulated low flows and the observed data. Post-calibration, this
550 alignment intensified. The VIC model tended to underestimate the low flows. After
551 calibration, the median bias improved from -23.6% to -9.9%, and with regionalization,
552 it was -11.7%. In contrast, Noah-MP began with an 11.20% overestimation in the

553 baseline, improved to 0.61% post-calibration, and was -9.5% after regionalization.
554 The outcomes underline the proficiency of both models for low flow prediction,
555 exhibiting enhanced competencies post-calibration and commendable performance
556 after regionalization.

557 **6. Discussion**

558 In this discussion, we summarize our key accomplishments in calibrating the two
559 hydrological models, examine our approach to choosing calibration objective
560 functions and metrics, and we consider lessons learned in model regionalization.

561 (a) Improved parameter sets

562 We generated calibrated parameter sets for the VIC and Noah-MP hydrological
563 models at 1/16° latitude-longitude scale across WUS. These calibrated parameter sets
564 are intended to facilitate the use of the two models for climate change and water
565 investigations across the region, among other applications. Our focus on calibrating
566 daily streamflow aligns with common practice in hydrology, providing a
567 comprehensive representation of catchment hydrology dynamics which should
568 enhance future understanding of hydrological phenomena and their spatial variations
569 across the region.

570 (b) Selection of calibration objective function

571 We used objective functions based on streamflow observations. We chose this
572 approach due to its applicability elsewhere, given the widespread accessibility of
573 streamflow observations as compared to alternative metrics such as soil moisture or
574 evapotranspiration (Demaria et al., 2007; Gao et al., 2018; Troy et al., 2008; Yadav et
575 al., 2007). While we acknowledge the potential of remote sensing products like
576 MODIS, SMAP, SMOS, ESA, and ALEXI to improve calibration efforts, especially
577 for variables like actual evapotranspiration (AET) and soil moisture (SM), we were
578 limited by the scarcity of observations for these variables. Future studies could,

579 nonetheless, leverage from the methods we've employed to incorporate additional
580 variables into the objective functions we used.

581 (c) Selection of calibration metric

582 We used the KGE metric applied to daily streamflow, which we chose for its
583 ability to address bias, correlation, and variability simultaneously (Knoben et al.,
584 2019). We also evaluated NSE and BIAS metrics, and found substantial
585 improvements in both models' performance after calibration when these metrics were
586 used in place of KGE (See Figures S2-3). Our assessment of high and low flow
587 reconstruction in Section 5 further validated our generated parameter sets. While we
588 used a single objective function due to data and computing constraints, incorporating
589 multiple objective functions is feasible in principle.

590 (d) Regionalization possibilities

591 We calibrated model parameters directly for individual basins, considering their
592 unique hydrological features, and then transferred these calibrated parameters to
593 similar basins based on similarity assessments. Alternative parameter transfer
594 strategies could be used within the same framework we employed (e.g., pedo-transfer
595 functions, e.g. Imhoff et al.,2020) or multiscale parameter regionalization (e.g.
596 Schweppe et al.,2022). We do note that our regionalization approach facilitates the
597 transfer of calibrated parameters to comparable regions, which could be explored in
598 future research.

599 **7. Conclusions**

600 Our intent was to develop a regional parameter estimation strategy for the VIC
601 and Noah-MP land surface schemes, and to apply it across the WUS region at the
602 HUC-10 catchment scale. We've described what we believe is a robust framework
603 that can be applied in future hydrological and climate change studies across the WUS,
604 and is applicable to other regions as well. Our key findings and conclusions are:

- 605 a) Our catchment scale calibration of the two models to 263 sites across WUS
606 resulted in major improvements in the performance of both models relative to
607 a priori parameters, but performance improvement was greatest for Noah-
608 MP – although this may be in part because VIC a priori parameters benefitted
609 from prior calibration and hence resulted in better baseline performance than
610 did a priori Noah-MP.
- 611 b) Both models performed best in more humid basins, mainly in the Pacific
612 Northwest and central to northern CA where runoff ratios are high. This is
613 consistent with previous results (e.g. Bass et al.,2023).
- 614 c) Post-calibration regional model performance improved for both models in
615 most areas, especially where the baseline KGE was low, such as southern CA
616 and the southeastern part of the study region.
- 617 d) VIC performance across all calibration basins generally was better than for
618 Noah-MP. However, Noah-MP performance benefitted more from
619 regionalization than did VIC, and ultimately post-regionalization VIC
620 performance was only slightly superior to that of Noah-MP.

621

622 **Data Availability statement**

623 The Livneh (2013) forcings are available at

624 <http://livnehpublicstorage.colorado.edu:81/Livneh.2013.CONUS.Dataset/>. The

625 extended forcings used in this study are available at <ftp://livnehpublicstorage.>

626 <colorado.edu/public/sulu>. The results are available online at

627 <https://figshare.com/s/66fe8305bff516e80f6f> .

628

629

630

631 **Author contribution**

632 LS and DL conceptualized the study. LS generated the dataset and analysis with

633 support of DL, MP and BB. LS drafted the manuscript with support of DL.

634

635 **Competing interests.** The contact author has declared that none of the authors has

636 any competing interests.

637

638 **References**

- 639 Adam, J.C. and Lettenmaier, D.P.: Adjustment of global gridded precipitation for
640 systematic bias, *J. Geophys. Res.*, 108(D9), 1-14, doi:10.1029/2002JD002499,
641 2003.
- 642 Adam, J.C., Clark, E.A. , Lettenmaier, D.P. and Wood, E.F.: Correction of Global
643 Precipitation Products for Orographic Effects, *J. Clim.*, 19(1), 15-38, doi:
644 10.1175/JCLI3604.1, 2006.
- 645 Anghileri, D., Voisin, N., Castelletti, A., Pianosi, F. , Nijssen, B. and Lettenmaier, D.P.:
646 Value of Long-Term Streamflow Forecasts to Reservoir Operations for Water
647 Supply in Snow-Dominated River Catchments. *Water Resources Research* 52:
648 4209–25, 2016.
- 649 Arsenault, R., and Brissette, F. P.: Continuous streamflow prediction in ungauged
650 basins: The effects of equifinality and parameter set selection on uncertainty in
651 regionalization approaches. *Water Resour. Res.*, 50, 6135–6153, [https://doi.org/](https://doi.org/10.1002/2013WR014898)
652 10.1002/2013WR014898, 2014.
- 653 Bass, B., Rahimi, S., Goldenson, N., Hall, A., Norris, J. and Lebow, Z.J.: Achieving
654 Realistic Runoff in the Western United States with a Land Surface Model Forced
655 by Dynamically Downscaled Meteorology. *Journal of Hydrometeorology*, 24(2),
656 269-283, 2023.
- 657 Beck, H. E., Roo, A. de and van Dijk, A. I. J. M.: Global maps of streamflow
658 characteristics based on observations from several thousand catchments. *J.*
659 *Hydrometeor.*, 16, 1478–1501, <https://doi.org/10.1175/JHM-D-14-0155.1>, 2015.
- 660 Bennett, A. R., Hamman, J. J. and Nijssen, B.: MetSim: A Python package for
661 estimation and disaggregation of meteorological data. *J. Open Source Software*,
662 5, 2042, <https://doi.org/10.21105/joss.02042>, 2020.
- 663 Beven, K.: Changing ideas in hydrology-the case of physically-based models. *Journal*

664 of Hydrology, 105(1-2), 157–172. [https://doi.](https://doi.org/10.1016/0022-1694(89)90101-7)
665 [org/10.1016/0022-1694\(89\)90101-7](https://doi.org/10.1016/0022-1694(89)90101-7), 1989.

666 Bohn, T. J., Livneh, B., Oyler, J. W., Running, S. W., Nijssen, B. and Lettenmaier, D.
667 P.: Global evaluation of MTCLIM and related algorithms for forcing of
668 ecological and hydrological models. *Agric. For. Meteor.*, 176, 38–49,
669 <https://doi.org/10.1016/j.agrformet.2013.03.003>, 2013.

670 Boucher, M.-A., and Ramos, M.-H.: Ensemble Streamflow Forecasts for Hydropower
671 Systems. In *Handbook of Hydrometeorological Ensemble Forecasting*, edited by
672 Q. Duan, F. Pappenberger, J. Thielen, A. Wood, H.L. Cloke, and J.C. Schaake, 1–
673 19. Berlin Heidelberg: Springer, 2018.

674 Burn, D. H., and Boorman, D. B.: Estimation of hydrological parameters at ungauged
675 catchments. *J. Hydrol.*, 143,429454, [https://doi.org/10.1016/0022-](https://doi.org/10.1016/0022-1694(93)90203-L)
676 [1694\(93\)90203-L](https://doi.org/10.1016/0022-1694(93)90203-L), 1993.

677 Cai, X., Yang, Z.-L. , David, C. H., Niu, G.-Y. and Rodell, M.: Hydrological
678 evaluation of the Noah-MP land surface model for the Mississippi River Basin. *J.*
679 *Geophys. Res. Atmos.*, 119, 23–38, <https://doi.org/10.1002/2013JD020792>, 2014.

680 California Department of Water Resources: California data exchange center: Daily
681 full natural flow for December 2022. California Department of Water Resources,
682 accessed 1 October 2021, [https://cdec.water.ca.gov/reportapp/javareports?name=](https://cdec.water.ca.gov/reportapp/javareports?name=FNF)
683 [FNF](https://cdec.water.ca.gov/reportapp/javareports?name=FNF), 2021.

684 Cao, Q., Mehran, A. , Ralph, F. M. and Lettenmaier, D. P.: The role of hydrological
685 initial conditions on atmospheric river floods in the Russian River basin. *J.*
686 *Hydrometeor.*, 20, 16671686, <https://doi.org/10.1175/JHM-D-19-0030.1>, 2019.

687 Cao, Q., Gershunov, A., Shulgina, T., Ralph, F. M. , Sun, N. and Lettenmaier, D. P.:
688 Floods due to atmospheric rivers along the U.S. West Coast: The role of
689 antecedent soil moisture in a warming climate. *J. Hydrometeor.*, 21, 1827–1845,

690 [https:// doi.org/10.1175/JHM-D-19-0242.1](https://doi.org/10.1175/JHM-D-19-0242.1), 2020.

691 Castiglioni, S., Lombardi, L., Toth, E. , Castellarin, A. and Montanari, A.: Calibration
692 of rainfall-runoff models in ungauged basins: A regional maximum likelihood
693 approach. *Advances in Water Resources*, 33(10), 1235–1242.
694 <https://doi.org/10.1016/j.advwatres.2010.04.009>, 2010.

695 Chen, F., and Dudhia, J.: Coupling an advanced land surface–hydrology model with
696 the Penn State–NCAR MM5 modeling system. Part I: Model implementation
697 and sensitivity. *Mon. Wea. Rev.*, 129, 569–585, [https://doi.org/10.1175/1520-](https://doi.org/10.1175/1520-0493(2001)129<0569:CAALSH>2.0.CO;2)
698 [0493\(2001\)129<0569:CAALSH>2.0.CO;2](https://doi.org/10.1175/1520-0493(2001)129<0569:CAALSH>2.0.CO;2), 2001.

699 Chen, F., and Coauthors: Modeling of land-surface evaporation by four schemes and
700 comparison with FIFE observations. *J. Geophys. Res.*, 101, 7251–7268,
701 <https://doi.org/10.1029/95JD02165>, 1996.

702 Cosby, B.J., Hornberger, G.M., Clapp, R.B. and Ginn, T.: A statistical exploration of
703 the relationships of soil moisture characteristics to the physical properties of soils.
704 *Water resources research*, 20(6), 682–690, 1984.

705 Demaria, E. M., Nijssen, B., & Wagener, T.: Monte Carlo sensitivity analysis of land
706 surface parameters using the Variable Infiltration Capacity model. *Journal of*
707 *Geophysical Research*, 112, D11113. <https://doi.org/10.1029/2006JD007534>,
708 2007.

709 Demirel, M. C., Mai, J., Mendiguren, G., Koch, J., Samaniego, L., and Stisen, S.:
710 Combining satellite data and appropriate objective functions for improved spatial
711 pattern performance of a distributed hydrologic model, *Hydrol. Earth Syst. Sci.*,
712 22, 1299–1315, <https://doi.org/10.5194/hess-22-1299-2018>, 2018.

713 Dickinson, R. E., Henderson-Sellers, A. & Kennedy, P. J.: Biosphere–Atmosphere
714 Transfer Scheme (BATS) version 1e as coupled to the NCAR Community
715 Climate Model. NCAR Tech. Note TN383+STR, NCAR, 1993.

716 Duan, Q., Sorooshian, S. and Gupta, V. : Effective and efficient global optimization
717 for conceptual rainfall-runoff models. *Water Resour. Res.*, 28, 1015–1031,
718 [https://doi.org/ 10.1029/91WR02985](https://doi.org/10.1029/91WR02985), 1992.

719 Environmental Protection Agency (EPA) Office of Water: Low Flow Statistics Tools:
720 A How-To Handbook for NPDES Permit Writers. EPA-833-B-18-001, 2018.

721 Falcone, J.: GAGES-II: Geospatial attributes of gages for evaluating streamflow. U.S.
722 Geological Survey, accessed 1 April 2021,
723 [https://water.usgs.gov/GIS/metadata/usgswrd/XML/ gagesII_Sept2011.xml](https://water.usgs.gov/GIS/metadata/usgswrd/XML/gagesII_Sept2011.xml), 2011.

724 Federal Institute of Hydrology: “SOSRHINE.”
725 http://sosrhine.euporias.eu/en/sosrhine_overview, 2020.

726 Fisher, R.A. and Koven, C.D.: Perspectives on the future of land surface models and
727 the challenges of representing complex terrestrial systems. *Journal of Advances*
728 *in Modeling Earth Systems*, 12(4), p.e2018MS001453, 2020.

729 Franchini, M., Galeati, G. and Berra S.: Global optimization techniques for the
730 calibration of conceptual rainfall-runoff models, *Hydrol. Sci. J.*, 43, 443 – 458,
731 1998.

732 Gao, H., Birkel, C., Hrachowitz, M., Tetzlaff, D., Soulsby, C., & Savenije, H. H.
733 (2018). A simple topography-driven, calibration-free runoff generation model.
734 *Hydrology and earth system sciences discussions.*,1–42.
735 <https://doi.org/10.5194/hess-2018-141>

736 Gochis, D. and Coauthors: Overview of National Water Model Calibration: General
737 strategy and optimization. National Center for Atmospheric Research, accessed 1
738 January 2023, 30 pp.,
739 https://ral.ucar.edu/sites/default/files/public/9_RafieeiNasab_CalibOverview_CU
740 *AHSI_Fall019_0.pdf*, 2019.

741 Gong, W., Duan, Q., Li, J., Wang, C., Di, Z., Dai, Y., et al.: Multi-objective parameter

742 optimization of common land model using adaptive surrogate modeling.
743 Hydrology and Earth System Sciences, 19(5), 2409–2425.
744 <https://doi.org/10.5194/hess-19-2409-2015>, 2015.

745 Gou, J., Miao, C., Duan, Q., Tang, Q., Di, Z., Liao, W., Wu, J. and Zhou, R.:
746 Sensitivity analysis-based automatic parameter calibration of the VIC model for
747 streamflow simulations over China. *Water Resources Research*, 56(1),
748 e2019WR025968, 2020.

749 Gupta, H. V., et al.: Decomposition of the mean squared error and NSE performance
750 criteria: Implications for improving hydrological modelling. *Journal of*
751 *Hydrology*, 377, 80-91,2009.

752 Holtzman, N.M., Pavelsky, T.M., Cohen, J.S., Wrzesien, M.L. and Herman, J.D.:
753 Tailoring WRF and Noah-MP to improve process representation of Sierra
754 Nevada runoff: Diagnostic evaluation and applications. *Journal of Advances in*
755 *Modeling Earth Systems*, 12(3), p.e2019MS001832, 2020.

756 Hussein, A.: Process-based calibration of WRF-hydro model in unregulated
757 mountainous basin in Central Arizona. M.S. thesis, Ira A. Fulton Schools of
758 Engineering, Arizona State University, 110 pp.,
759 [https://keep.lib.asu.edu/_flysystem/fedora/](https://keep.lib.asu.edu/_flysystem/fedora/c7/224690/Hussein_asu_0010N_19985.pdf)
760 [c7/224690/Hussein_asu_0010N_19985.pdf](https://keep.lib.asu.edu/_flysystem/fedora/c7/224690/Hussein_asu_0010N_19985.pdf), 2020.

761 Imhoff, R.O., Van Verseveld, W.J., Van Osnabrugge, B. and Weerts, A.H.: Scaling
762 point-scale (pedo) transfer functions to seamless large-domain parameter
763 estimates for high-resolution distributed hydrologic modeling: An example for
764 the Rhine River. *Water Resources Research*, 56(4), p.e2019WR026807,2020.

765 Kimball, J. S., Running, S. W. and Nemani, R. R.: An improved method for
766 estimating surface humidity from daily minimum temperature. *Agric. For.*
767 *Meteor.*, 85, 87–98, [https:// doi.org/10.1016/S0168-1923\(96\)02366-0](https://doi.org/10.1016/S0168-1923(96)02366-0), 1997.

768 Lahmers, T.M., et al.: Evaluation of NOAA national water model parameter
769 calibration in semiarid environments prone to channel infiltration. *Journal of*
770 *Hydrometeorology*, 22(11), 2939-2969, 2021.

771 Li, D., Lettenmaier, D. P., Margulis, S. A. and Andreadis, K.: The role of rain-on-
772 snow in flooding over the conterminous United States. *Water Resour. Res.*, 55,
773 8492–8513, <https://doi.org/10.1029/2019WR024950>, 2019.

774 Liang, X., Lettenmaier, D. P., Wood, E. F. and Burges S. J. : A simple hydrologically
775 based model of land surface water and energy fluxes for general circulation
776 models, *J. Geophys. Res.*, 99(D7), 14415–14428, doi:10.1029/94JD00483, 1994.

777 Livneh B, Rosenberg, E.A., Lin, C., Nijssen, B., Mishra, V., Andreadis, K., Maurer,
778 E.P. and Lettenmaier, D.P.: A long-term hydrologically based data set of land
779 surface fluxes and states for the conterminous United States: Updates and
780 extensions, *Journal of Climate*, doi:10.1175/JCLI-D-12-00508.1, 2013.

781 Maidment, D.R.: Conceptual Framework for the National Flood Interoperability
782 Experiment. *Journal of the American Water Resources Association* 53: 245–57,
783 2017.

784 Mascaro, G., Hussein, A., Dugger, A. and Gochis, D.J.: Process-based calibration of
785 WRF-Hydro in a mountainous basin in southwestern US. *Journal of the*
786 *American Water Resources Association*, 59(1), 49-70, 2023.

787 Mendoza, P.A., Clark, M.P., Mizukami, N., Newman, A.J., Barlage, M., Gutmann,
788 E.D., Rasmussen, R.M., Rajagopalan, B., Brekke, L.D. and Arnold, J.R.: Effects
789 of hydrologic model choice and calibration on the portrayal of climate change
790 impacts. *Journal of Hydrometeorology*, 16(2), 762-780, 2015.

791 Miller, D.A. and White, R.A.: A conterminous United States multilayer soil
792 characteristics dataset for regional climate and hydrology modeling. *Earth*
793 *interactions*, 2(2), pp.1-26, 1998.

794 Mizukami, N., Clark, M. P., Newman, A. J., Wood, A. W., Gutmann, E. D., Nijssen,
795 B. , Rakovec, O. and Samaniego, L. :Towards seamless large-domain parameter
796 estimation for hydrologic models. *Water Resour. Res.*, 53, 8020–8040, [https://](https://doi.org/10.1002/2017WR020401)
797 doi.org/10.1002/2017WR020401, 2017.

798 Naeni, M.R., Analui, B., Gupta, H.V., Duan, Q. and Sorooshian, S.. Three decades of
799 the Shuffled Complex Evolution (SCE-UA) optimization algorithm: Review and
800 applications. *Scientia Iranica*, 26(4), 2015-2031, 2019.

801 Natural Resources Conservation Service: SNOTEL (Snow Telemetry) Data. USDA.
802 <https://www.nrcs.usda.gov/wps/portal/wcc/home/>, 2023.

803 Niu, G.-Y., Yang, Z.-L. , Dickinson, R. E. , Gulden, L. E. and Su, H.: Development of
804 a simple groundwater model for use in climate models and evaluation with
805 gravity recovery and climate experiment data. *J. Geophys. Res.*, 112, D07103,
806 <https://doi.org/10.1029/2006JD007522>, 2007.

807 Niu, G. Y., Yang, Z. L., Dickinson, R. E., & Gulden, L. E.: A simple
808 TOPMODEL-based runoff parameterization (SIMTOP) for use in global climate
809 models. *Journal of Geophysical Research: Atmospheres*, 110(D21), 2005.

810 Niu, G.-Y., and Coauthors: The community Noah land surface model with
811 multiparameterization options (Noah-MP): 1. Model description and evaluation
812 with local-scale measurements. *J. Geophys. Res.*, 116, D12109,
813 <https://doi.org/10.1029/2010JD015139>, 2011.

814 NOAA (National Oceanic and Atmospheric Administration): National Water Model:
815 Improving NOAA’s Water Prediction Services, 2016.

816 Oubeidillah, A. A., Kao, S.-C., Ashfaq, M. , Naz, B. S. and Tootle, G.: A large-scale,
817 high-resolution hydrological model parameter data set for climate change impact
818 assessment for the conterminous US. *Hydrology and Earth System Sciences*,
819 18(1), 67–84. <https://doi.org/10.5194/hess-18-67-2014>, 2014.

820 Prata, A.J.: A new long-wave formula for estimating downward clear-sky radiation at
821 the surface. Quarterly Journal of the Royal Meteorological Society, 122(533),
822 1127-1151, 1996.

823 Poissant, D., Arsenault, A. and Brissette, F. : Impact of parameter set dimensionality
824 and calibration procedures on streamflow prediction at ungauged catchments. J.
825 Hydrol. Reg. Stud., 12,220–237, <https://doi.org/10.1016/j.ejrh.2017.05.005>, 2017.

826 Qi, W.Y., Chen, J. , Li, L. , Xu, C.-Y. , Xiang, Y.-h. , Zhang, S.-B. and Wang, H.-M.:
827 Impact of the number of donor catchments and the efficiency threshold on
828 regionalization performance of hydrological models. J. Hydrol., 601, 126680,
829 <https://doi.org/10.1016/j.jhydrol.2021.126680>, 2021.

830 Raff, D., Brekke, L. , Werner, K. , Wood, A. and White. K.: Short-Term Water
831 Management Decisions: User Needs for Improved Climate, Weather, and
832 Hydrologic Information. U.S. Bureau of Reclamation.
833 <https://www.usbr.gov/research/st/roadmaps/WaterSupply.pdf>, 2013.

834 Razavi, T., and Coulibaly, P.: An evaluation of regionalization and watershed
835 classification schemes for continuous daily streamflow prediction in ungauged
836 watersheds. Can. Water Resour. J., 42,2–20,
837 <https://doi.org/10.1080/07011784.2016.1184590>, 2017.

838 Rajsekhar, D., Singh, V.P. and Mishra, A.K., 2015. Hydrologic drought atlas for Texas.
839 Journal of Hydrologic Engineering, 20(7), p.05014023.

840 Schaake, J. C., Koren, V. I., Duan, Q.-Y., Mitchell, K., & Chen, F.: Simple water
841 balance model for estimating runoff at different spatial and temporal scales.
842 Journal of Geophysical Research, 101(D3), 7461–7475.
843 <https://doi.org/10.1029/95JD02892>, 1996.

844 Schaperow J.R, Li, D., Margulis, S.A., Lettenmaier D.P. :A near-global, high
845 resolution land surface parameter dataset for the variable infiltration capacity

846 model. *Scientific Data*. Aug 11;8(1):216, 2021.

847 Schwappe, R., Thober, S., Müller, S., Kelbling, M., Kumar, R., Attinger, S., and
848 Samaniego, L.: MPR 1.0: a stand-alone multiscale parameter regionalization tool
849 for improved parameter estimation of land surface models, *Geosci. Model Dev.*,
850 15, 859–882, <https://doi.org/10.5194/gmd-15-859-2022>, 2022.

851 Sharma, P. and Machiwal, D.: Streamflow forecasting: overview of advances in data-
852 driven techniques. *Advances in Streamflow Forecasting*, 1-50.
853 <https://doi.org/10.1016/B978-0-12-820673-7.00013-5>, 2021

854 Shi, X., Wood, A.W. and Lettenmaier, D.P. : How essential is hydrologic model
855 calibration to seasonal streamflow forecasting? *Journal of Hydrometeorology*,
856 9(6), 1350-1363, 2008.

857 Sofokleous, I., Bruggeman, A., Camera, C. and Eliades, M.: Grid-based calibration of
858 the WRF-Hydro with Noah-MP model with improved groundwater and
859 transpiration process equations. *Journal of Hydrology*, 617, 128991 , 2023

860 Su, L., Cao, Q. , Xiao, M., Mocko, D. M., Barlage, M. , Li, D. , Peters-Lidard, C. D.
861 and Lettenmaier, D. P.: Drought variability over the conterminous United States
862 for the past century. *J. Hydrometeor.*, 22, 1153–1168,
863 <https://doi.org/10.1175/JHM-D-20-0158.1>, 2021.

864 Su, L., Cao, Q. , Shukla, S., Pan, M. and Lettenmaier, D.P.: Evaluation of Subseasonal
865 Drought Forecast Skill over the Coastal Western United States. *Journal of*
866 *Hydrometeorology*, 24(4), 709-726, 2023.

867 Tangdamrongsub, N.: Comparative Analysis of Global Terrestrial Water Storage
868 Simulations: Assessing CABLE, Noah-MP, PCR-GLOBWB, and GLDAS
869 Performances during the GRACE and GRACE-FO Era. *Water*, 15(13), p.2456,
870 2023.

871 Thornton, P. E., and Running, S. W.: An improved algorithm for estimating incident

872 daily solar radiation from measurements of temperature, humidity, and
873 precipitation. *Agric. For. Meteor.*, 93, 211–228, [https://doi.org/10.1016/S0168-](https://doi.org/10.1016/S0168-1923(98)00126-9)
874 1923(98) 00126-9, 1999.

875 Tolson, B. A., and Shoemaker, C. A.: Dynamically dimensioned search algorithm for
876 computationally efficient watershed model calibration. *Water Resour. Res.*, 43,
877 W01413, <https://doi.org/10.1029/2005WR004723>, 2007.

878 Troy, T. J., Wood, E. F. and Sheffield, J.: An efficient calibration method for
879 continental-scale land surface modeling. *Water Resources Research*, 44, W09411.
880 <https://doi.org/10.1029/2007WR006513>, 2008

881 USWRC: Guidelines for determining flood flow frequency. Bulletin 17B of the
882 Hydrology Subcommittee, 183 pp., [https://](https://water.usgs.gov/osw/bulletin17b/dl_flow.pdf)
883 water.usgs.gov/osw/bulletin17b/dl_flow.pdf, 1982.

884 Yang, Y., Pan, M., Beck, H.E. , Fisher, C.K., Beighley, R.E. , Kao, S.C. , Hong, Y. and
885 Wood, E.F.: In quest of calibration density and consistency in hydrologic
886 modeling: Distributed parameter calibration against streamflow characteristics.
887 *Water Resources Research*, 55(9), 7784-7803, 2019.

888 Yadav, M., Wagener, T., & Gupta, H. (2007). Regionalization of constraints on
889 expected watershed response behavior for improved predictions in ungauged
890 basins. *Advances in Water Resources*, 30(8), 1756–1774.
891 <https://doi.org/10.1016/j.advwatres.2007.01.005>

892 Zheng, H., Yang, Z.-L. , Lin, P. , Wei, J. , Wu, W.-Y., Li, L. , Zhao, L. and Wang, S. :
893 On the sensitivity of the precipitation partitioning into evapotranspiration and
894 runoff in land surface parameterizations. *Water Resour. Res.*, 55, 95–111,
895 <https://doi.org/10.1029/2017WR022236>, 2019.

896 Zink M, Mai J, Cuntz M, Samaniego L. Conditioning a hydrologic model using
897 patterns of remotely sensed land surface temperature. *Water Resources Research*.

898 2018 Apr;54(4):2976-98.

899